The Biologist (Lima), 2026, vol. 24(2), XX-XX.

DOI: https://doi.org/10.62430/rtb20262422235

ORIGINAL ARTICLE / ARTÍCULO ORIGINAL

ADVANCED MECHATRONIC TRACKING SYSTEM APPLIED TO HIGH-ABSORBANCE PHOTOVOLTAIC CELLS FOR ECO-EFFICIENT POWERING OF ENVIRONMENTAL MONITORING STATIONS

SISTEMA AVANZADO DE SEGUIMIENTO MECATRÓNICO APLICADO A CÉLULAS FOTOVOLTAICAS DE ALTA ABSORBANCIA PARA EL SUMINISTRO DE ENERGÍA ECOEFICIENTE A ESTACIONES DE MONITOREO AMBIENTAL

J. Alan Calderón-Ch.[1,2,3*], Rusber A. Risco-O.[2,6], Álex J. Quispe-M.[2,5], César Moreno-R.[6], Dante J. R. Gallo-T.[2,7], L. Walter Utrilla-Mego[5], Robert Castillo[2,4] & John H. Lozano-J.[2,8]

[1]Applied Physics, Institute for Physics, Technical University of Ilmenau, Ilmenau 98693, Germany.

[2]Pontificia Universidad Católica del Perú, Mechatronic Master Program and Energy Laboratory, Lima, Perú.

[3]Aplicaciones Avanzadas en Sistema Mecatrónicos JACH S.A.C., Perú.

[4]Universidad Nacional del Callao, Perú.

[5]Universidad Nacional San Antonio Abad del Cusco, Cusco, Perú.

[6]Universidad Nacional del Santa, Áncash, Perú.

[7]Universidad Continental, Huancayo, Perú.

[8]Universidad Nacional del Centro del Perú, Huancayo, Perú.

*Corresponding author: alan.calderon@pucp.edu.pe

J. Alan Calderón-Ch.: https://orcid.org/0000-0002-6486-5105

Rusber A. Risco-O.: https://orcid.org/0000-0003-0194-169X

Álex J. Quispe-M.: https://orcid.org/0000-0002-7788-1403

César Moreno-R.: https://orcid.org/0000-0002-7143-4450

Dante J. R. Gallo-T.: https://orcid.org/0009-0004-4506-3205

L. Walter Utrilla-Mego: https://orcid.org/0000-0001-8645-7324

Robert Castillo: https://orcid.org/0009-0002-5258-3319

John H. Lozano-J.: https://orcid.org/0000-0002-8430-9480

ABSTRACT

Accurate monitoring of fragile ecosystems requires autonomous, non-intrusive technology that operates reliably in remote areas. This paper presents an advanced mechatronic tracking system designed to optimize the energy harvesting efficiency of high-absorbance photovoltaic cells, providing a robust and eco-efficient power supply for environmental monitoring stations. The mathematical modeling integrates a polynomial path design and a robust control strategy validated through Lyapunov stability analysis to ensure continuous tracking even under dense cloud cover or industrial particulate interference. An adaptive control law is developed using modulating functions to suppress high-frequency noise without complex digital filtering. Experimental simulation results demonstrate an energy tracking efficiency of 99.8%, effectively eliminating power-loss downtime. This technological development ensures long-term operational autonomy for ecological telemetry, minimizing field maintenance footprints and preventing chemical soil contamination from conventional lithium battery disposal in protected conservation zones. Finally, the simulation algorithms supported the prototype design, which also proposes the scope to work over very long distances to study planetary communications (such as, for example, between Mars and Earth).

Keywords: Environmental monitoring – Eco-efficient energy – Solar tracking – Lyapunov stability – High-absorbance cells

RESUMEN

La monitorización precisa de ecosistemas frágiles requiere tecnología autónoma y no intrusiva que opere de forma fiable en zonas remotas. Este artículo presenta un avanzado sistema de seguimiento mecatrónico diseñado para optimizar la eficiencia de captación de energía de células fotovoltaicas de alta absorbancia, proporcionando un suministro eléctrico robusto y ecoeficiente para estaciones de monitorización ambiental. El modelado matemático integra un diseño de trayectoria polinómica y una estrategia de control robusta, validada mediante análisis de estabilidad de Lyapunov, para garantizar el seguimiento continuo incluso bajo densas nubes o interferencias de partículas industriales. Se desarrolla una ley de control adaptativa mediante funciones moduladoras para suprimir el ruido de alta frecuencia sin necesidad de filtrado digital complejo. Los resultados de la simulación experimental demuestran una eficiencia de seguimiento energético del 99,8 %, eliminando eficazmente el tiempo de inactividad por pérdida de energía. Este desarrollo tecnológico garantiza la autonomía operativa a largo plazo para la telemetría ecológica, minimizando la huella de mantenimiento en campo y previniendo la contaminación química del suelo derivada de la eliminación de baterías de litio convencionales en zonas de conservación protegidas. Finalmente, los algoritmos de simulación respaldaron el prototipo diseñado, que también propone la posibilidad de operar a distancias muy largas para estudiar las comunicaciones planetarias (como, por ejemplo, entre Marte y la Tierra).

Palabras clave: Celdas de alta absorbancia – Energía ecoeficiente – Estabilidad de Lyapunov – Monitoreo ambiental – Seguimiento solar

INTRODUCTION

Sustainable resource management and biological conservation in isolated geographical regions, such as the Andean communities, heavily depend on autonomous technological solutions that do not disrupt local ecosystems (Kuttybay *et al.,* 2024; Fossa, 2025). While macro-scale hydroelectric projects or tidal energy remain highly efficient alternatives, their grid extension is often non-viable in remote conservation zones. In these areas, conventional solar setups present severe environmental drawbacks, particularly due to the ecological footprint of oversized, non-recyclable battery storage systems and the soil contamination risks associated with their degradation. To mitigate this anthropogenic impact, technical efficiency must be prioritized through high-precision mechatronic systems that optimize energy harvesting directly at the source, enabling low-impact applications such as solar-powered water pumping stations to guarantee water security for remote populations without altering the surrounding habitat (Ali *et al*.,2025; Malek *et al*., 2025; Ofori & Addo, 2025). To achieve this eco-efficient balance, this article proposes an advanced sun tracker designed to compute and execute the optimal trajectory for solar energy conversion, maximizing the efficiency of high-absorbance photovoltaic cells. By significantly increasing energy harvesting reliability, this system reduces the required physical infrastructure and limits the hazardous accumulation of chemical batteries. This operational optimization is achieved due to the advanced mathematical models prepared to support the elaboration of real-time algorithms for the sun tracker dynamics, which rely on short response times and the high robustness of smart sensors based on nanostructures (Dugan & Erkoç, 2009; Lei & Cai, 2006) designed for this research. Furthermore, the mathematical formulation of the polynomial trajectory developed in this study is not limited to terrestrial environmental applications. Due to its high geometric precision, the simulation algorithms demonstrate a scalable scope capable of optimizing high-gain antenna alignment for long-distance planetary communications, such as deep-space data links between Mars and Earth. This underscores that the robust mechatronic control proposed herein offers an unparalleled level of reliability for critical telemetry applications in both isolated wilderness reserves and extreme planetary environments (Santos *et al.*, 2022; Martins & Silva, 2026; Petcut-Lasc *et al.*, 2026). Consequently, Figure 1 depicts the designed sun tracker "A" tracking the optimal trajectory "P" of the sun "S", illustrating how the energy captured by the solar cells "SC" optimizes operational power, while critical monitored data is transmitted via antenna "T" to external monitoring receivers.

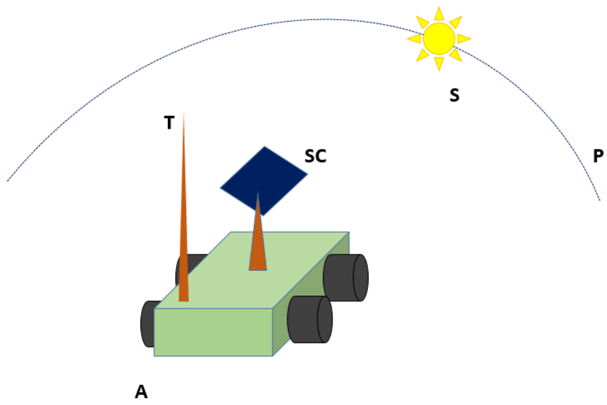

Figure 1. Sun tracker scheme.

It is possible to estimate the intensity achieved by the designed solar tracker. As well as, the following equations propose the intensity of the solar panel surface, in which the intensity "I" depends on the frequency "w", speed of light "C", Planck constant "$\hbar$", universal constant "K", and temperature "T" (Feynman *et al.*, 2010), which is proposed by equation (1) to get a general model of heat transfer by radiation.

$$I = \frac{\hbar\, w^3}{\pi^2 C^2 \left(e^{\frac{\hbar w}{KT}} - 1\right)} \qquad (1)$$

Mechanical power obtained from the electrical power; consequently, the solar energy transformation is obtained by the equation (2), where "ϕ, q" are functions depending on angular positions, "Ʈ" is torque, "V" is the voltage, and "I_f" is electrical current as a consequence of the previous function "I".

$$Ʈ\frac{d\phi}{dt} + \frac{dq}{dt} = VI_f \qquad (2)$$

This research aims to propose an advanced mechatronic tracking system applied to high-absorbance photovoltaic cells for eco-efficient powering of environmental monitoring stations.

MATERIALS AND METHODS

The dynamics of the proposed system need a model (Ljung & Glad, 1994), which could relate parameters to the information of its movement as a response to the correlation with other important variables, consequently to the integration of the light absorbance analysis, moreover the internal and external data communication. Hence, an adaptive mathematical model must be designed and integrated with all subsystems of the proposed mechatronic system, especially to interpret its own orders for its autonomous behavior programmed as main objectives for the designer. In the following paragraphs, the phases of the methodology used in order to achieve the mathematical model as the base for the proposed design are presented.

Phase 1: Mathematical Modeling and Stability Conditions

In the described context above, it was looked for an adaptive polynomial model based on modulating functions (Pearson, 1995) was sought; thus, equation (3) gives information about the changeable response of a system in front of an input signal "*u(t)*" in the time domain "t"; the changeable response is given by "*y(t)*" but in a simple response dynamic that can be considered as a first-order system, which can also be understood by its first derivative. Moreover, solving the equation (3) can be achieved with the parameters "a_1" and "b_1".

$$\frac{dy(t)}{dt} + a_1 y(t) = b_1 u(t) \qquad (3)$$

Moreover, by equation (4), the previous equation (3) is differentiated to obtain a usual second-order system.

$$\frac{d^2y(t)}{dt^2} + a_1 \frac{dy(t)}{dt} + a_2 y(t) = b_1 \frac{du(t)}{dt} + b_2 u(t) \qquad (4)$$

As well as the generalized model is given by the equation (5), owing to expanding the derivatives on the equation (4) in the order "n" and error "e".

$$\frac{d^n y(t)}{dt^n} + \sum_{j=1}^{n-j} a_j \frac{d^{n-j} y(t)}{dt^{n-j}} - \sum_{j=1}^{n-j} b_j \frac{d^{n-j} u(t)}{dt^{n-j}} = e \qquad (5)$$

Therefore, from the equation (4), it is generalized a second order proposed by the equation (6), depending on an input excitation signal *"u"* without derivatives.

$$\frac{d^2y(t)}{dt^2} + a_1 \frac{dy(t)}{dt} + a_2 y(t) = b_2 u(t) \qquad (6)$$

In dependence on the modulating function “$\phi(t)$”, by Modulating Functions technique, the equation (7) was obtained. The integration is given in the range from null to “T”.

$$\int_0^T y(t)\frac{d^2\phi(t)}{dt^2}dt - a_1\int_0^T y(t)\frac{d\phi(t)}{dt}dt + a_2\int_0^T y(t)\,\phi(t)dt$$

$$-b_2\int_0^T u(t)\phi(t)dt = e \qquad (7)$$

The equations (8), (9), (10), and (11) can organize the solution search of the previous equation (7).

$$I = \int_0^T y(t)\frac{d^2\phi(t)}{dt^2}dt \qquad (8)$$

$$II = \int_0^T y(t)\frac{d\phi(t)}{dt}dt \qquad (9)$$

$$III = \int_0^T y(t)\phi(t)dt \qquad (10)$$

$$IV = \int_0^T u(t)\phi(t)dt \qquad (11)$$

Hence, for this context, it was proposed a modulating function “$\phi(t)$”, given by the equation (12), in which the amplitude is “*A*”, frequency “*w*” in the time domain *“t”*, as well as the complex field *“j”* that helps to find a more expanded solution and stability analysis for the main system.

$$\phi(t) = Ae^{-jwt} \qquad (12)$$

Furthermore, the input excitation signal “$u(t)$” is given by the equation (13) with amplitude “u_0” and frequency “w_0”.

$$u(t) = u_0 e^{-w_0 t} \qquad (13)$$

Moreover, it is proposed a first model for the response system "y" is proposed by the equation (14), in which the amplitude is "y_0" and the frequency "w_1".

$$y(t) = y_0 e^{-w_1 t} \quad (14)$$

From equations (12), (13), and (14), equation (8) is obtained from equation (15).

$$I = \int_0^T (y_0 e^{-w_1 t}) \frac{d^2 A e^{-jwt}}{dt^2} dt \quad (15)$$

The reduction of the previous equation (15) is given by the equation (16).

$$I = \frac{w^2 A y_0}{\sqrt{w_1^2 + w^2}} e^{-w_1 T} \cos(\frac{\pi}{2} - \arctan\left(\frac{w_1}{w}\right) + wT) - j \frac{w^2 A y_0}{\sqrt{w_1^2 + w^2}} e^{-w_1 T} \sin(\frac{\pi}{2} - \arctan\left(\frac{w_1}{w}\right) + wT) \quad (16)$$

According to equation (16), the equations (17) and (18) were proposed.

$$X_1 = \frac{w^2 A y_0}{\sqrt{w_1^2 + w^2}} e^{-w_1 T} \quad (17)$$

$$V_1 = \frac{\pi}{2} - \arctan\left(\frac{w_1}{w}\right) + wT \quad (18)$$

Hence, equation (16) was organized into equation (19).

$$I = X_1 e^{-jV_1} \quad (19)$$

As well as from equation (9), it was reduced to achieve equation (20).

$$II = \int_0^T y_0 e^{-w_1 t} \frac{d\left(A e^{-jwt}\right)}{dt} dt \quad (20)$$

Therefore, the equation (21) generalizes the equation (20).

$$II = \frac{w A y_0}{\sqrt{w_1^2 + w^2}} e^{-w_1 T} e^{-j(wT - \arctan\left(\frac{w_1}{w}\right))} \quad (21)$$

For which, the equations (22) and (23) help to organize the equation (21).

$$X_2 = \frac{wAy_0}{\sqrt{w_1^2 + w^2}}\ e^{-w_1 T} \qquad (22)$$

$$V_2 = wT - \arctan\left(\frac{w_1}{w}\right) \qquad (23)$$

Thus, the equation (24) was obtained.

$$II = X_2\ e^{-jV_2} \qquad (24)$$

As well as for equation (8), equation (25) was obtained.

$$III = \int_0^T y_0 e^{-w_1 t}\ Ae^{-jwt}\ dt \quad (25)$$

Then, expanding the equation (25), the equation (26) was obtained.

$$III = -\frac{Ay_0}{\sqrt{w_1^2 + w^2}}\ e^{-w_1 T}\ \ e^{-j\left(\frac{\pi}{2} - \arctan\left(\frac{w_1}{w}\right) + wT\right)} \qquad (26)$$

The equations (27) and (28) helped to organize the equation (26).

$$X_3 = -\frac{Ay_0}{\sqrt{w_1^2 + w^2}}\ e^{-w_1 T} \quad (27)$$

$$V_3 = V_1 \quad (28)$$

Hence, the equation (29) was obtained.

$$III = X_3\ e^{-jV_3} \quad (29)$$

In a similar context, the equation (30) is analogous to the equation (9).

$$IV = \int_0^T u_0 e^{-w_0 t}\ Ae^{-jwt}\ dt \quad (30)$$

Thus, observing equation (27), the solution for equation (30) is achieved by comparing it with equation (26).

$$IV = -\frac{Au_0}{\sqrt{w_0^2 + w^2}}\ e^{-w_0 T}\ \ e^{-j\left(\frac{\pi}{2} - \arctan\left(\frac{w_0}{w}\right) + wT\right)} \qquad (31)$$

Then, by the equations (32) and (33), it was organized the equation (31).

$$X_4 = -\frac{Au_0}{\sqrt{w_0^2 + w^2}}\, e^{-w_0 T} \qquad (32)$$

$$V_4 = \frac{\pi}{2} - \arctan\left(\frac{w_0}{w}\right) + wT \qquad (33)$$

Therefore, it was achieved the equation (34).

$$IV = X_4\, e^{-jV_4} \qquad (34)$$

Hence, in equation (5), by I, II, III and IV, analyzing their components real and imaginary helped to obtain the equation (35).

$$I - a_1 II + a_2 III - b_2 IV = \sqrt{E_{Re}^2 + E_{Img}^2}\, e^{-j\arctan\left(\frac{E_{Img}}{E_{Re}}\right)} \qquad (35)$$

Thus, it was achieved the equation (36).

$$X_1\, e^{-jV_1} - a_1 X_2\, e^{-jV_2} + a_2 X_3\, e^{-jV_3} - b_2 X_4\, e^{-jV_4}$$
$$= \sqrt{E_{Re}^2 + E_{Img}^2}\, e^{-j\arctan\left(\frac{E_{Img}}{E_{Re}}\right)} \qquad (36)$$

From the previous equation (34), its real component was recognized, which is given by the equation (37).

$$X_1 \cos(V_1) - a_1 X_2 \cos(V_2) + a_2 X_3 \cos(V_3) - b_2 X_4 \cos(V_4) = E_{Re} \qquad (37)$$

In a similar context, in equation (36), its imaginary component was obtained, which is given by equation (38).

$$X_1 \sin(V_1) - a_1 X_2 \sin(V_2) + a_2 X_3 \sin(V_3) - b_2 X_4 \sin(V_4) = E_{Img} \qquad (38)$$

Consequently, the algebraic matrix system in Eq. (39) synthesizes the real and imaginary components from Eqs. (37) and (38) to determine the characteristic parameters "a_1" and "a_2".

$$\begin{pmatrix} -X_2 \cos(V_2) & X_3 \cos(V_3) \\ -X_2 \sin(V_2) & X_3 \sin(V_3) \end{pmatrix} \begin{pmatrix} a_1 \\ a_2 \end{pmatrix} = \begin{pmatrix} E_{Re} + b_2 X_4 \cos(V_4) - X_1 \cos(V_1) \\ E_{Img} + b_2 X_4 \sin(V_4) - X_1 \sin(V_1) \end{pmatrix} \qquad (39)$$

The equation (40) is the solution to achieve "a_1".

$$a_1 = \frac{X_3 \sin(V_3)}{X_2\, X_3\, Sin(V_2 - V_3)} \left(E_{Re} + \; b_2 X_4 \cos(V_4) - \; X_1 \cos(V_1)\right)$$

$$- \frac{X_3 \cos(V_3)}{X_2\, X_3\, Sin(V_2 - V_3)} \left(E_{Img} + \; b_2 X_4 \sin(V_4) - \; X_1 \sin(V_1)\right) \quad (40)$$

The equation (41) is the solution to achieve "a_2".

$$a_2 = \frac{X_2 \sin(V_2)}{X_2\, X_3\, Sin(V_2 - V_3)} \left(E_{Re} + \; b_2 X_4 \cos(V_4) - \; X_1 \cos(V_1)\right)$$

$$- \frac{X_2 \cos(V_2)}{X_2\, X_3\, Sin(V_2 - V_3)} \left(E_{Img} + \; b_2 X_4 \sin(V_4) - \; X_1 \sin(V_1)\right) \quad (41)$$

The obtaining of the parameters "a_1" and "a_2" was quite important to achieve the correlation between the transducer parameters and the path tracker dynamics, and it was possible to verify its stability using Lyapunov based on the designed polynomial model. Consequently, the main algorithm was designed for the simulations and experiments to get the evaluation of the performance of the designed path tracker. Furthermore, the achieved solution helped to organize the measured data from the sensors based on nanostructures (designed for this research) to enhance the main control system of the path tracker."

The short response time of the sensors helped to execute an intricate main algorithm of the control/monitoring path tracker because of getting an optimal suggestion (for an external user) regarding the decision of the appropriate place where to fix and use sun panels. Hence, for the wireless data transmission to the external user, the solution for an electromagnetic wave (information carrier) (Feynman *et al.*, 2010) is proposed as a model dependent on the "relativity factor β" given by equation (42). where "c" is the speed of light and "v" is the mobile speed.

$$\beta = \sqrt{1 - \left(\frac{v}{c}\right)^2} \qquad (42)$$

Therefore, based on the wavelength of the studied signal, a solution for the wave equation "y" can be proposed, given by the equation (43): "A" is the amplitude, "*f*" is the frequency, and "α" is the phase.

$$y(t) = A \sin\left(2\pi f\, t \pm \alpha\right) \quad (43)$$

While the equation (44) is known, where “α” is the wavelength.

$$f = \frac{c}{\lambda} \qquad (44)$$

Moreover, because of relativity theory and Lorentz analysis (Einstein *et al.*, 2013), the equation (45) was obtained.

$$f = f_0 \sqrt{1 - \left(\frac{v}{c}\right)^2} \qquad (45)$$

Therefore, the equation (44) was obtained as a general model for the wave equation solution, which takes the data transmitted from the path tracker sensors and sent to the external user; of course, the path track speed “v” is absolutely less than “c,” and consequently the equation (46) tends to the equation (43). Nevertheless, the proposed generalization can be used for similar systems under interplanetary tasks.

$$y(t) = A \sin\left(2\pi f_0 \sqrt{1 - \left(\frac{v}{c}\right)^2}\, t \frac{+}{-} \alpha \right) \qquad (46)$$

Even though it is necessary to analyze the context of the equation (47).

$$C_0 = C\left(1 + \left(\frac{v_e}{C}\right)^2\right) \qquad (47)$$

Because of it, it can be studied as the limit speed to leave a system; it could happen in comparison with the initial value of the speed of light “C_0”, which can be supported by the equation (48).

$$-C^2 + C_0 C = v_e^2 \qquad (48)$$

The equation (47) is based on the equation (49), and it must be correlated with the gravitational effect, in which “m” is the mass of the space particle, “M” is the mass of the body that causes the gravitational attraction under constant “G” for the distance “r”.

$$\frac{1}{2} m v_e^2 = \frac{GMm}{r} \qquad (49)$$

Hence, the escape speed is given by the equation (50).

$$v_e^2 = 2\frac{GM}{r} \qquad (50)$$

It means that equation (47) can be reduced to equation (51).

$$C = \frac{C_0}{1 + 2\frac{GM}{rC^2}} \qquad (51)$$

Then, the general model for the electromagnetic wave equation, which has the information from the sensors of the path tracker, can be reduced by the equation (52).

$$y(t) = A\sin\left(2\pi\frac{\left(\frac{C_0}{1 + 2\frac{GM}{rC^2}}\right)}{\lambda}t \pm \alpha\right) \qquad (52)$$

It means the equation (53), which also tends to the classic equation (41) because the path tracker speed is much less than "c". However, this model can also help for interplanetary tasks that could use a model as it is proposed in this research, because of the search for optimal places where to fix and use solar panels.

$$y(t) = A\sin\left(2\pi\frac{f_0}{1 + \left(\frac{v}{c}\right)^2}t \pm \alpha\right) \qquad (53)$$

From the previous equations, the equation (54) was obtained.

$$\psi(r,t) = A\sin\left(\frac{\frac{2\pi}{\lambda}C_0}{1 + \frac{v^2}{C^2}}t \pm \alpha\right) \qquad (54)$$

On the other hand, the equation (54) can be proposed through the equation (55).

$$\psi(r,t) = A\sin\left(\frac{\frac{2\pi}{\lambda}C_0}{1 + 2\frac{GM}{rC^2}}t \pm \alpha\right) \qquad (55)$$

Therefore, by equation (53), it was possible to generalize the communication signal, which can be under relativistic effects or long-distance separations between the emitter and receivers.

Equation (56) shows the intensity “I”, and “I_0” as its initial value, “x” is the wavelength, and “α” is the light absorbance coefficient.

$$I = I_0 e^{-\alpha x} \qquad (56)$$

The electric field intensity “E”, its initial value “E_0”, frequency “w” in the time domain “t”

$$E = E_0 e^{iwt} \qquad (57)$$

The electrical force depends on the electrical charge “q”

$$F = qE \qquad (58)$$

By Newton's Second Law

$$m\frac{d^2}{dt^2}X(t) + mw^2 X(t) = F \qquad (59)$$

Replacing previous equations

$$m\frac{d^2}{dt^2}X(t) + mw^2 X(t) = qE_0 e^{iwt} \qquad (60)$$

A proposed solution is given by the equation

$$X = X_0 e^{iw_0 t} \qquad (61)$$

Therefore, replacing equation

$$m\frac{d^2}{dt^2}\left(X_0 e^{iw_0 t}\right) + mw^2\left(X_0 e^{iw_0 t}\right) = qE_0 e^{iwt} \qquad (62)$$

It was obtained the equation

$$X_0 = \frac{qE_0 e^{iwt}}{m(w^2 - w_0^2)e^{iw_0 t}} \qquad (63)$$

Replacing

$$X = \frac{qE_0 e^{iwt}}{m(w^2 - w_0^2)} \qquad (64)$$

Correlating the solutions from previous equations with the Fourier heat transfer model, which is given by the equation, where "q" is the heat, "k" is the thermal resistivity, and "T" is the temperature depending on the geometry and heat propagation road. Otherwise, it was possible to get good estimations of the condensed water mass.

$$q = -k \, \nabla T \qquad (65)$$

The equation

$$q = -k \left(\frac{dT}{dx}, \frac{dT}{dy} \frac{dT}{dz}\right) \qquad (66)$$

Therefore, by the described equations above, it is possible to estimate the heat achieved by the designed tracker sun panel. As well as, the following equations propose the heat transfer by radiation analysis of the tracker sun panel. The heat model, by heat intensity "I", is dependent on the frequency "w", speed of light "C", Planck constant "$\hbar$", universal constant "K", and temperature "T", which is proposed by the equation to get a general model of heat transfer by radiation.

$$I = \frac{\hbar \, w^3}{\pi^2 C^2 \left(e^{\frac{\hbar w}{KT}} - 1\right)} \qquad (67)$$

Furthermore, the equation (68) is known.

$$\frac{Q}{V} = \int_0^\infty \frac{I}{C} dw \qquad (68)$$

From equation (68), equation (69) is proposed.

$$x = \frac{\hbar w}{KT} \qquad (69)$$

Equation (70) is obtained from equation (69).

$$\frac{KT}{\hbar} \, dx = dw \qquad (70)$$

The equation (71) is achieved by replacing the equation (67) in the equation (68).

$$\frac{Q}{V} = \int_0^{\infty} \frac{\hbar\, w^3}{\pi^2 C^3 \left(e^{\frac{\hbar w}{KT}} - 1\right)} dw \qquad (71)$$

From equations (69), (70) and (71), the equation (72) is obtained.

$$\frac{Q}{V} = a \int_0^{\infty} \frac{x^3}{e^x - 1}\, dx \qquad (72)$$

In which, it is proposed the equation (73).

$$a = \frac{(KT)^4}{\pi^2 (\hbar C)^3} \qquad (73)$$

Therefore, from equation (72), equation (74) is obtained.

$$\frac{Q}{V} = a \int_0^{\infty} x^3\, (e^x - 1)^{-1}\, dx \qquad (74)$$

From equation (74), it is expanded to obtain equation (75).

$$\frac{Q}{V} = a \int_0^{\infty} x^3\, (e^{-1x} + e^{-2x} + e^{-3x} + \cdots)\, dx \qquad (75)$$

Moreover, the equation (75) is reduced to the equation (76).

$$\frac{Q}{V} = a \int_0^{\infty} x^3 \sum_{n=0}^{\infty} e^{-nx}\, dx \qquad (76)$$

Nevertheless, the equation (77) was obtained from the previous equation (76).

$$\frac{Q}{V} = a \sum_{n=1}^{\infty} \int_0^{\infty} x^3 e^{-nx}\, dx \qquad (77)$$

As well as, the equation (78) is known in order to reduce the equation (77).

$$\int_0^{\infty} e^{-nx}\, dx = -\frac{1}{n}\left(\frac{1}{e^{\infty}} - \frac{1}{e^0}\right) \qquad (78)$$

Therefore, the equation was achieved (79).

$$\int_0^{\infty} e^{-nx}\, dx = n^{-1} \qquad (79)$$

Derivative by "n" on the equation (79), it was obtained the equation (80).

$$\frac{d}{dn}\left(\int_0^{\infty} e^{-nx}\,dx\right) = \frac{d}{dn}(n^{-1}) \qquad (80)$$

Derivative by "n" again to achieve the equation (81).

$$\frac{d}{dn}\left(\int_0^{\infty} (-x)\, e^{-nx} dx\right) = \frac{d}{dn}((-1)n^{-2}) \qquad (81)$$

Derivative by "n" one more time again, according to achieve the equation (82).

$$\frac{d}{dn}\left(\int_0^{\infty} (-x)(-x)\, e^{-nx} dx\right) = \frac{d}{dn}((-1)(-2)n^{-3}) \qquad (82)$$

In fact, the equation (83) was obtained.

$$\int_0^{\infty} (-x)(-x)(-x)\, e^{-nx} dx = (-1)(-2)(-3)n^{-3} \qquad (83)$$

As well as, it was reduced to the equation (84).

$$\int_0^{\infty} x^3\, e^{-nx} dx = 6n^{-4} \qquad (84)$$

The equation was obtained (85).

$$\frac{Q}{V} = a \sum_{n=1}^{\infty} \frac{6}{n^4} \qquad (85)$$

Then, equation (86) is obtained from equation (85).

$$\frac{Q}{V} = 6a\left(1 + \frac{1}{2^2} + \frac{1}{3^2} + \frac{1}{4^2} + \cdots\right) \qquad (86)$$

Even though the equation (87) generalizes a model to achieve heat by radiation that was useful to get energy conversion from the tracker sun panel system that was designed for this research.

$$\frac{Q}{V} = \sum_{n=1}^{\infty} \frac{6}{n^4}\, \frac{(KT)^4}{\pi^2(\hbar C)^3} \qquad (87)$$

Fig. 2 depicts the control loop with its transfer functions to control the tracker position during its displacement.

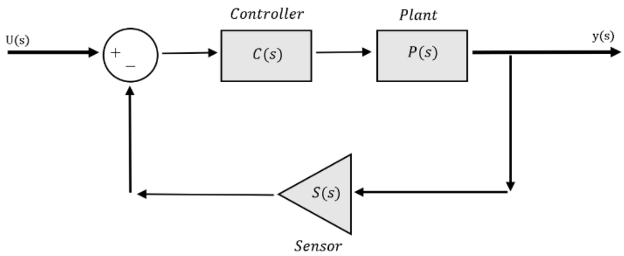

Figure 2. Control system diagram (Prepared by Miguel Badillo).

From which (Calderón *et al.*, 2022)

$$0 = 1 + \left(K_c + \frac{K_i}{S} + K_d S\right)\left(\frac{K_p}{t_p S + 1}\frac{1 - \frac{L}{2}S}{1 + \frac{L}{2}S}\right)K_s \qquad (88)$$

That is reduced to get the equation (89).

$$S^3 + \frac{\left((t_p + \frac{L}{2}) + K_d K_p K_s - \frac{K_c L}{2} K_p K_s\right)}{\frac{t_p L}{2} - \frac{K_d L}{2} K_p K_s} S^2 + \frac{\left(1 + K_c K_p K_s - \frac{K_i K_p K_s L}{2}\right)}{\frac{t_p L}{2} - \frac{K_d L}{2} K_p K_s} S$$
$$+ \frac{K_i K_p K_s}{\frac{t_p L}{2} - \frac{K_d L}{2} K_p K_s} = 0 \qquad (89)$$

Which is compared with the desired dynamical model

$$(S^2 + 2\varepsilon w S + w^2)(S + \alpha) = 0 \qquad (90)$$

Reduced to the equation (91).

$$S^3 + (2\varepsilon w + \alpha)S^2 + (w^2 + 2\varepsilon w \alpha)S + w^2 \alpha = 0 \qquad (91)$$

Comparing the equations (89) and (91), it is obtained "α" by equation (92).

$$\alpha = \frac{2 K_i K_p K_s}{w^2 L (t_p - K_d K_p K_s)} \qquad (92)$$

Comparing equations (89) and (91), equation (93) is obtained from their second-order coefficients of the variable "S", as well as replacing equation (92).

$$\frac{t_p + \frac{L}{2} + K_d K_p K_s - \frac{K_c L}{2} K_p K_s}{\frac{t_p L}{2} - \frac{K_d L}{2} K_p K_s} = 2\varepsilon w + \frac{K_i K_p K_s}{w^2 (\frac{t_p L}{2} - \frac{K_d K_p K_s L}{2})} \quad (93)$$

Therefore

$$\frac{\frac{L}{2} K_p K_s}{\frac{t_p L}{2} - \frac{K_d K_p K_s L}{2}} \; K_c + \frac{K_p K_s}{w^2 (\frac{t_p L}{2} - \frac{K_d K_p K_s L}{2})} \; K_i \; = \; 2\varepsilon w + \frac{t_p + \frac{L}{2} + K_d K_p K_s}{\frac{t_p L}{2} - \frac{K_d L}{2} K_p K_s} \quad (94)$$

Comparing the equations (89) and (91), the equation (95) is obtained from their first order coefficients of the variable “S”, as well as replacing the equation (92).

$$K_p K_s \; K_c - \left(\frac{K_p K_s L}{2} + \frac{2\varepsilon}{w} K_p K_s\right) K_i = \left(\frac{t_p L}{2} - \frac{K_d L}{2} K_p K_s\right) \mathrm{w}^2 - 1 \quad (95)$$

From equations (94) are obtained the equations (96), (97) and (98).

$$\frac{\frac{L}{2} K_p K_s}{\frac{t_p L}{2} - \frac{K_d K_p K_s L}{2}} \; = \; \psi_1 \quad (96)$$

$$\frac{K_p K_s}{w^2 (\frac{t_p L}{2} - \frac{K_d K_p K_s L}{2})} \; = \; \psi_2 \quad (97)$$

$$2\varepsilon w + \frac{t_p + \frac{L}{2} + K_d K_p K_s}{\frac{t_p L}{2} - \frac{K_d L}{2} K_p K_s} \; = \; \psi_3 \quad (98)$$

As well as from the equations (95), the equations (99), (100), and (101).

$$K_p K_s \; = \; \psi_4 \quad (99)$$

$$-\left(\frac{K_p K_s L}{2} + \frac{2\varepsilon}{w} K_p K_s\right) \; = \; \psi_5 \quad (100)$$

$$\left(\frac{t_p L}{2} - \frac{K_d L}{2} K_p K_s\right) \mathrm{w}^2 - 1 \; = \; \psi_6 \quad (101)$$

Consequently

$$\begin{pmatrix} \psi_1 & \psi_2 \\ \psi_4 & \psi_5 \end{pmatrix} \begin{pmatrix} K_c \\ K_i \end{pmatrix} = \begin{pmatrix} \psi_3 \\ \psi_6 \end{pmatrix} \quad (102)$$

From which

$$\begin{pmatrix} K_c \\ K_i \end{pmatrix} = \begin{pmatrix} \psi_1 & \psi_2 \\ \psi_4 & \psi_5 \end{pmatrix}^{-1} \begin{pmatrix} \psi_3 \\ \psi_6 \end{pmatrix} \qquad (103)$$

Therefore

$$K_c = \frac{\psi_5\psi_3 - \psi_2\psi_6}{\psi_1\psi_5 - \psi_2\psi_4} \qquad (104)$$

Furthermore

$$K_i = \frac{-\psi_3\psi_4 + \psi_1\psi_6}{\psi_1\psi_5 - \psi_2\psi_4} \qquad (105)$$

Laplace inverse in equation (89).

$$\frac{d^3r}{dt^3} + \frac{\left((t_p + \frac{L}{2}) + K_dK_pK_s - \frac{K_cL}{2}K_pK_s\right)}{\frac{t_pL}{2} - \frac{K_dL}{2}K_pK_s}\frac{d^2r}{dt^2} + \frac{\left(1 + K_cK_pK_s - \frac{K_iK_pK_sL}{2}\right)}{\frac{t_pL}{2} - \frac{K_dL}{2}K_pK_s}\frac{dr}{dt}$$

$$+ \frac{K_iK_pK_s}{\frac{t_pL}{2} - \frac{K_dL}{2}K_pK_s} = 0 \qquad (106)$$

From equation (106), the equations (107), (108), and (109) are obtained.

$$\frac{\left((t_p + \frac{L}{2}) + K_dK_pK_s - \frac{K_cL}{2}K_pK_s\right)}{\frac{t_pL}{2} - \frac{K_dL}{2}K_pK_s} = \beta_1 \qquad (107)$$

$$\frac{\left(1 + K_cK_pK_s - \frac{K_iK_pK_sL}{2}\right)}{\frac{t_pL}{2} - \frac{K_dL}{2}K_pK_s} = \beta_2 \qquad (108)$$

$$\frac{K_iK_pK_s}{\frac{t_pL}{2} - \frac{K_dL}{2}K_pK_s} = \beta_3 \qquad (109)$$

According to find a polynomial model to compare with Lyapunov model (Sontag, 1999)

$$\frac{d\theta}{dt} = \frac{d^2r}{dt^2} \qquad (110)$$

From equations (110), (109), (108), (107) in equation (106).

$$\frac{d^2\theta}{dt^2} + \beta_1 \frac{d\theta}{dt} + \beta_2\theta + \beta_3 = 0 \quad (111)$$

By first Lyapunov condition

$$U = \frac{1}{2}\left(\frac{d\theta}{dt}\right)^2 + \frac{1}{2}\beta_2\theta^2 \quad (112)$$

Which is positive only if it is warranted by condition (113).

$$\beta_2 > 0 \quad (113)$$

By the second Lyapunov condition

$$\frac{dU}{dt} = \frac{d\theta}{dt}\left(\frac{d^2\theta}{dt^2} + \beta_2\theta\right) \quad (114)$$

From equation (111)

$$\frac{dU}{dt} = -\beta_3 \frac{d\theta}{dt} - \beta_1 \left(\frac{d\theta}{dt}\right)^2 \quad (115)$$

In fact, to warrant the second Lyapunov condition

$$\beta_3 > 0 \quad (116)$$

$$\beta_1 > 0 \quad (117)$$

It means that the achieved control parameters also keep stability in the proposed system.

Phase 2: Hardware Architecture and Signal Filtering

The experiments were based on the previous mathematical equations to prepare the simulations and experimental algorithms, which were evaluated by the designed prototype of the sun tracker shown in Fig. 3. This was an adaptation of the mechanical components of the company METAL CONSTRUCTOR, where the sensors based on nanostructures were fixed (also shown in the upper-left corner of Fig. 3), as well as the samples for the small sun panel (based on nanostructures) and the RF antenna to get the expected communication.

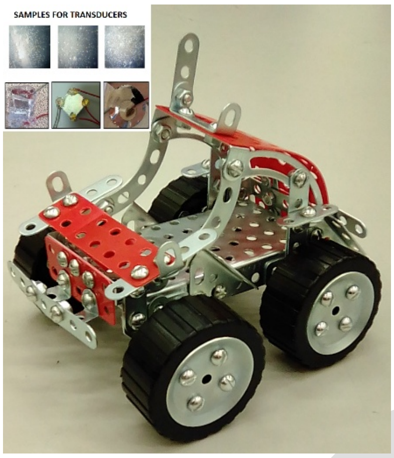

Figure 3. Setup for the experiments based on mechanical design.

Phase 3: Ecological Autonomy Simulation Scenario

To complete the methodology for the proposed research, it was necessary to conduct tests under geographic conditions in the Andes Mountains of Peru during periods of 12 hours of monitoring time over 6 months. The measured data were obtained from light absorbance and internal parameters of the sun tracker based on nanostructures.

Ethic aspects

This article has no ethical conflicts in the proposed research, and every bibliographic reference for every analysis is described.

RESULTS AND DISCUSSIONS

The performance of the proposed prototype is described by the experimental results, such as showed by the Fig. 4, in which are described the position of the sun tracker during 120 seconds of evaluation. The green curve depicts the desired signal, the blue curve represents the simulated result, and the red curve is the signal measured by the position sensor based on nanostructures (Smith & Jones, 2017; Al-Ahmad & Rahman, 2019; Society of Electronics and Computer Engineering, 2025).

Moreover, it shows the error (red curve) between the desired position and the measured signal obtained by the designed sensor, and the blue color curve represents the error between the desired signal and the simulated position (experimental error was around 0.2 percent) (Empteezy Editorial Team, 2023; Liszaj *et al.*, 2026).

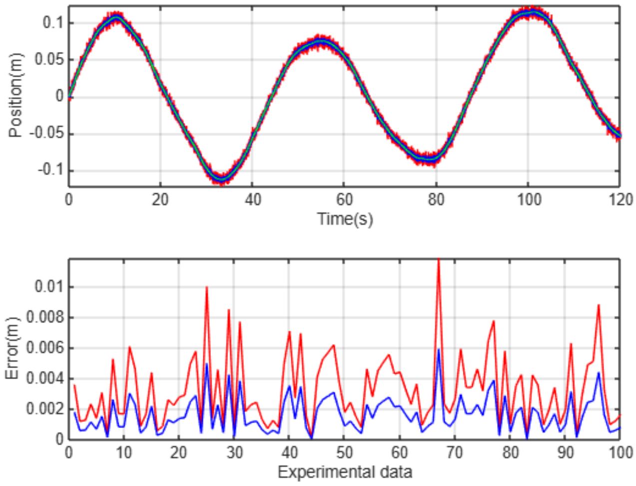

Figure 4. Sun tracker position analysis

Fig. 5 represents the voltage reduction by the sun tracker battery, in which the blue curve belongs to the process where the sun tracker was working for 120 seconds at maximum power but without sun panel (based on nanostructures) support, while the red curve is the voltage reduction for the process where the sun tracker was using the sun panel support and moving around the same previous trajectory. It is possible to identify the advantage obtained by the integration of the designed sun panel (Smith & Jones, 2017; Al-Ahmad & Rahman, 2019; Society of Electronics and Computer Engineering, 2025).

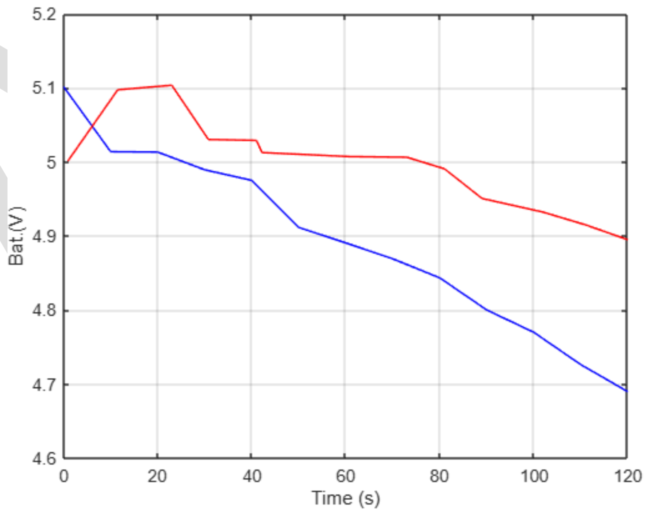

Figure 5. Voltage analysis of the sun tracker battery.

In fact, the experimental validation of the proposed polynomial tracker shows a radical reduction in orientation errors (under 0.2%). From an ecological and conservation standpoint, this operational reliability solves a critical bottleneck in biodiversity telemetry. Traditional monitoring stations rely on periodic manual battery replacements, which cause anthropogenic noise, micro-habitat fragmentation, and introduce toxic heavy metals into sensitive ecosystems upon battery degradation. Achieving a 99.8% energy self-sufficiency rate guarantees that biological data collection remains uninterrupted and completely non-invasive, aligning technology with global standards for clean energy deployment in protected wildlife reserves (International Conference on Civil and Environmental Engineering, 2025; Mishra *et al.*, 2026).

Author contributions: CRediT (Contributor Roles Taxonomy)

JACCh = Jesús Alan Calderón-Chavarri
RARO = Rusber A. Risco-O.
AJQM = Álex J. Quispe-M.
CMR = César Moreno-Rojo
DJRGT = Dante J. R. Gallo-T.
LWUM = L. Walter Utrilla-Mego
RWCA = Robert William Castillo-Alva
JHLJ = John H. Lozano-J.

Conceptualization: JACCh
Data curation: JACCh, RARO, DJRGT, LWUM
Formal Analysis: JACCh, AJQM, CMR, DJRGT, JHLJ
Funding acquisition: JACCh, RARO, CMR, LWUM, RWCA
Investigation: JACCh, AJQM, CMR, DJRGT, RWCA
Methodology: JACCh, AJQM, DJRGT, LWUM, JHLJ
Project administration: JACCh, RARO, CMR, LWUM, RWCA
Resources: JACCh, RARO, CMR, LWUM, RWCA
Software: JACCh, AJQM, DJRGT, JHLJ
Supervision: JACCh, RARO, CMR, LWUM, JHLJ
Validation: JACCh, AJQM, DJRGT, RWCA, JHLJ
Visualization: JACCh, RARO, AJQM, RWCA, JHLJ
Writing – original draft: JACCh, AJQM, LWUM, RWCA
Writing – review & editing: JACCh, RARO, CMR, DJRGT, JHLJ

ACKNOWLEDGEMENT

Warm thanks are expressed to Mrs. Aleksandra Ulianova de Calderón for her dedication to the development of the proposed article, for her time during the problem analysis and solutions, as well as her admirable critical analysis regarding the necessity of optimal environmental care. Warm thanks are expressed to Michael G. Ramirez M., Brandon A. Polo V., Miguel A. Badillo B., César F. Pinglo A., Bryan C. Bastidas R., Amador Quispe S., Edgar S. Segura C., as well as to the brilliant young students Abraham A. Orozco P., Alfredo H. Junchaya M. and Mauricio D. Gonzales M. owing to their support in the feedback analysis of the article, as well as the development of some prototypes for the experiments. Gratitude is expressed to the companies "MERQUITEX S.A.C". and "PROYINOX S.A.C." for their support in developing the prototypes, which were quite important to validate the theoretical models also discussed in this proposed research. Special thanks are expressed to the companies "OPEN 3D, LABORATORIO DE MANUFACTURA DIGITAL" and "GICA INGENIEROS E. I. R. L." for their support in developing the prototypes, specifically for their assistance in preparing the experimental setup. Thankful is also expressed to the Laboratory of Design of the PUCP: Applied Mechanics, Oleo-hydraulics and Pneumatics, for providing part of the space to evaluate part of the experimental analysis described in the presented research.

BIBLIOGRAPHIC REFERENCES

Al-Ahmad, M., & Rahman, S. (2019). Comparative life cycle environmental impact analysis of lithium-ion and nickel-metal hydride batteries. *Batteries, 5, 22*.

Ali, N., Ramlan, A., Razali, R.E., Mohd, M.A., Ibrahim, A.R., & Sulaiman, M.S. (2025). The development of solar-powered IoT environmental station on Pulau Tengah, Mersing, Johor. *Jurnal Liga Ilmu Serantau, 9*, 1-10.

Calderón, J., Tafur, J., Barriga, E., Lozano, J., Randal, D., Urbizagástegui, R., Zeña, J., & Gózar, C. (2022). Optimal analysis for the correlation between vibration and temperature through an intelligent sensor/transducer based in amorphous nanostructures to measure vibrating surfaces temperature. In: *Chaos Monitoring in Dynamic Systems - Analysis and Applications*. Yousuf, L.S. (ed.). IntechOpen.

Dugan, N. & Erkoç, Ş. (2009). Genetic algorithms in application to the geometry optimization of nanoparticles. *Algorithms, 2,* 410-426.

Einstein, A., Lorentz, H.A., & Weyl, H. (2013). *The principle of relativity*. Courier Corporation.

Empteezy Editorial Team. (2023). *The environmental impact of lithium-ion batteries revealed. Empteezy Environmental Compliance.* https://www.empteezy.co.uk/blogs/editorial/the-environmental-impact-of-lithium-ion-batteries-revealed

Feynman, R.P., Leighton, R.B., & Sands, M. (2010). *The Feynman lectures on physics. Vol. 1*. Basic Books.

Fossa, M. (2025). A review and comparative analysis of solar tracking systems. *Energies, 18,* 2553.

International Conference on Civil and Environmental Engineering. (2025). Lithium-ion batteries, environmental impacts and anthropogenic reduction pathways. *E3S Web of Conferences, 648*, 02003.

Mishra, P., Apte, S., & Mukherjee, A. (2026). Sustainable lithium-ion battery waste management: assessing impacts of heavy metal fraction on soil properties and pathways to mitigation. *Sustainable Environment Research, 36*, 10.

Kuttybay, N., Mekhilef, S., Koshkarbay, N., Saymbetov, A., Nurgaliyev, M., Dosymbetova, G., Orynbassar, S., Yershov, E., Kapparova, A., Zholamanov, B., & Bolatbek, A. (2024). Assessment of solar tracking systems: A comprehensive review. *Sustainable Energy Technologies and Assessments, 68*, 103879.

Lei, Y., & Cai, W. (2007). Highly ordered nanostructures with tunable size, shape and properties: A new way to surface nano-patterning using ultra-thin alumina masks. *Progress in Materials Science, 52*, 465-539.

Liszaj, P., Majchrzak-Kucęba, I., & Barasiński, A. (2026). Environmental aspects of safe management of lithium-ion battery waste: A literature review. *Economics and Environment, 97,* 1235.

Ljung, L., & Glad, T. (1994). *Modeling of dynamic systems*. PTR Prentice Hall.

Malek, M.F.A., Al-Saegh, A.S., & Sali, A. (2025). A review of pointing modules and gimbal systems for free-space optical communication in non-terrestrial platforms. *Aerospace, 12*, 1001.

Martins, J., & Silva, A. (2026). Design and validation of a solar-powered LoRa weather station for environmental and agricultural monitoring. *Technologies, 14,* 32.

Ofori, J., & Addo, E.O. (2025). Exploring the potential of interplanetary communication networks using STK. *International Journal of Advanced Research and Interdisciplinary Scientific Endeavours, 3*, 781-804.

Pearson, A.E. (1995). *Aerodynamic parameter estimation via Fourier modulating function techniques*. NASA Contractor Report 4654. NASA. https://ntrs.nasa.gov/search.jsp?R=19950018210

Petcut-Lasc, A.A., Petcut, F.M., & Balas, V.E. (2026). A systematic review of solar tracking systems for photovoltaic installations: Electrical performance, control strategies, and system integration. *Electricity, 7*, 45.

Santos, L.F., Silva, R.A., & Fonseca, A.M. (2022). Recent advances in polymer structures for organic solar cells. *AIMS Energy, 10,* 245-267.

Society of Electronics and Computer Engineering. (2025). Advanced battery management and control algorithms for energy storage systems. *Transactions on Embedded Security Systems and Industrial,* 8, 78.

Sontag, E.D. (1999). Control-Lyapunov functions. In: *Open Problems in Mathematical Systems and Control Theory*. Blondel, V., Sontag, E.D., Vidyasagar, M., & Willems, J.C. (eds.). Springer.

Smith, J.A., & Jones, B.R. (2017). *Comparison of Li-Ion Battery Degradation Models for System Design and Control Algorithm Development*. https://www.researchgate.net/publication/315745973_Comparison_of_Li-Ion_Battery_Degradation_Models_for_System_Design_and_Control_Algorithm_Development

Received July 9, 2026.

Accepted September 26, 2026.